Acta Crystallographica Section D
Biological Crystallography
ISSN 0907-4449

The mechanism of high-pressure-induced ordering in a macromolecular crystal

Tianwei Lin,[a]* Wilfried Schildkamp,[b] Keith Brister,[b] Peter C. Doerschuk,[c] Maddury Somayazulu,[d] Ho-kwang Mao[e] and John E. Johnson[a]

[a]Department of Molecular Biology and Center for Integrative Molecular Biosciences, The Scripps Research Institute, 10550 North Torrey Pines Road, La Jolla, CA 92037, USA, [b]The University of Chicago, Consortium for Advanced Radiation Sources, 5640 South Ellis Avenue, Chicago, IL, 60637, USA, [c]School of Electrical and Computer Engineering, Purdue University, West Lafayette, IN 47907, USA, [d]HPCAT, Advanced Photon Source, Argonne National Laboratory, Argonne, IL 60439, USA, and [e]Geophysical Laboratory, Carnegie Institute of Washington, 5251 Broad Branch Road NW, Washington, DC 20015, USA

Correspondence e-mail: twlin@scripps.edu

Received 24 August 2004
Accepted 3 January 2005

A previous study showed that the diffraction from cubic crystals of an icosahedral virus, cowpea mosaic virus (CPMV), was dramatically improved under elevated hydrostatic pressure. This use of pressure may have a significant impact on structural biology if it is found to be generally applicable. There were two types of cubic crystals assigned in either an *I*23 or *P*23 space group. They show the same rhombic dodecahedral morphology at atmospheric pressure. The crystals assigned to the *I*23 space group diffracted X-rays to higher resolution than those with *P*23 space group. The assignment of *P*23 space group was owing to the presence of reflections with indices of $h + k + l = (2n + 1)$ (odd reflections), which are forbidden in space group *I*23. Analysis of the odd reflections from the *P*23 crystals at atmospheric pressure showed that they can originate from a rotational disorder in the *I*23 crystals. The odd reflections were eliminated with the application of 3.5 kbar of pressure, which transformed the crystals from the apparently primitive cell to the body-centered *I*23 space group with dramatic improvement in diffraction. A mechanistic model is proposed to describe the induction of order by rectifying the imperfection, which is consistent with the experimental data.

1. Introduction

High-quality macromolecular crystals are the prerequisite for the determination of high-resolution structures by X-ray crystallography. However, macromolecular crystals are often grown with defects, which is a major impediment in structural biology. Previously, it was demonstrated that the diffraction from the crystals of an icosahedral plant virus, cowpea mosaic virus (CPMV), was improved with the elevation of hydrostatic pressure (Fourme *et al.*, 2002). To determine the general applicability of the phenomenon (Fig. 1), an understanding of the pressure-induced ordering is required.

CPMV is a member of the *Comovirus* family, a group of icosahedral plant viruses similar to mammalian *Picornaviruses*. They have a bipartite positive-sense single-stranded RNA genome packaged in an icosahedral capsid formed by 60 copies of a 24 kDa and 37 kDa

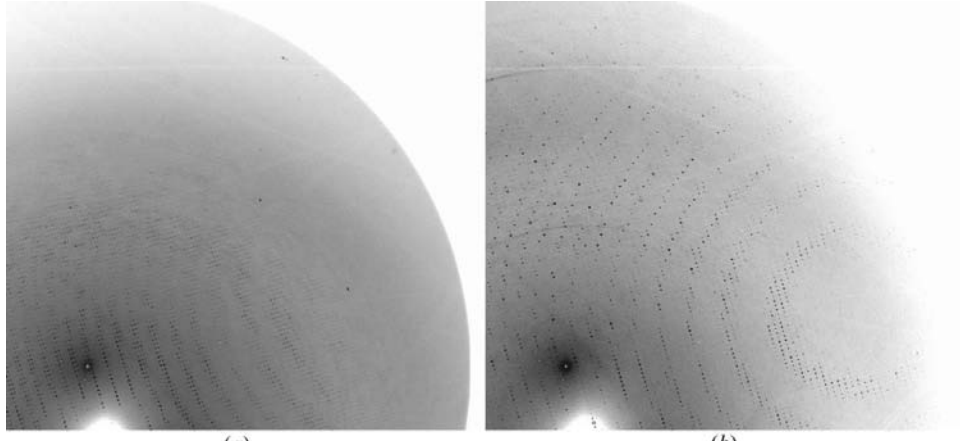

Figure 1
Pressure-induced ordering in a CPMV crystal. (*a*) Diffraction at atmospheric pressure. The limit of the diffraction is about 3 Å and the pattern is consistent with *P*23 space group. (*b*) Ramping of the pressure to 3.5 kbar dramatically improves the diffraction from the same crystal to the edge of the detector, corresponding to the resolution of 2.1 Å. The space group is converted to *I*23.

protein (Lomonossoff & Johnson, 1991). For structure determination by X-ray crystallography, crystals with a rhombic dodecahedral morphology were obtained and the cubic *I*23 space group (a = 317.0 Å) was assigned. The structure was determined to 3.5 Å resolution (Stauffacher *et al.*, 1987) and was later refined to 2.8 Å resolution (Lin *et al.*, 1999).

The previous structures were determined by merging reflections from multiple crystals. However, not all of the crystals strictly conformed to the *I*23 space group. In some crystals, reflections with indices of $h + k + l = (2n + 1)$ (odd reflections) were clearly present and these are forbidden in the *I*23 space group. Space group *P*23 was assigned, as it was consistent with the diffraction patterns with the primitive reflections even though there is no reasonable packing model for icosahedral particles in this space group. The odd reflections from these diffraction patterns were ignored and the data were integrated in space group *I*23. This was not detrimental to the structure determination, probably owing to the high-quality phases obtained from the phase refinement incorporating the fivefold non-crystallographic symmetry. However, by ignoring the odd reflections, not only was some structural information lost, but the origin of the odd reflections was also not addressed. Here, we report the investigation of the origin of the primitive reflections by analyzing data acquired at atmospheric pressure and at a pressure of 3.5 kbar (1 bar = 10^5 Pa). We show that the observed breakdown in *I*23 symmetry can be explained by a small rotation of the particle at the origin relative to body-centered particle.

2. Material and methods

2.1. Crystallization and cryogenic data collection at atmospheric pressure

CPMV was propagated, purified and crystallized according to established protocols (Lin *et al.*, 1999). The crystals were transferred to, and briefly submerged in, a cryo-preservation solution [100 m*M* potassium phosphate pH 7.0, 100 m*M* NH_4SO_4, 1.5%(*w*/*v*) PEG 8000, 30%(*v*/*v*) 2-methyl-2,4-pentanediol] and promptly flash-cooled under gaseous nitrogen at 100 K. The data were obtained at beamline 14-BM-C of BioCARS at the Advanced Photon Source. The detector was an ADSC Quantum 4 CCD, with 188 mm linear dimension, and the wavelength was 1.0 Å. The crystal-to-detector distance was 400 mm and the radiation was focused on the detector plane. The oscillation was 1° and the exposure time was 10 s. The focal spot size was measured at 160 µm in the horizontal direction and 300 µm in the vertical direction. The size of the beam at the sample position was 600 µm horizontally and 350 µm vertically. This set-up exposes the entire crystal volume and reduces radiation damage, as described by Wikoff *et al.* (2000).

These data were measured in two passes so that both strong and weak reflections were measured adequately without overloads. 90° of data were collected to 4 Å resolution for the analysis in space groups of lower symmetry.

Table 1
Data acquired at atmospheric pressure.

Data set No.	Space group	No. of reflections	Completeness (%)	R_{merge} (%)
1	*I*23	39488	92.7	5.5
2	*P*23	83268	96.2	11.4
	*I*23	42345	98.5	8.4
3	*P*23	83693	97.8	10.6
	*I*23	42522	99.8	9.7
4	*P*23	82983	97.8	9.6
	*I*23	42436	99.6	8.6
5	*P*23	85109	99.9	8.6
	*I*23	42474	99.7	8.4
6	*P*23	85196	99.9	12.7
	*I*23	42589	99.9	9.1

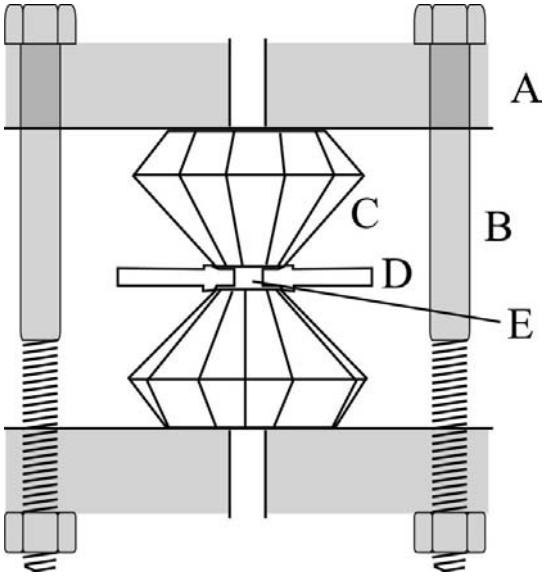

Figure 2
Schematic diagram of a diamond anvil cell (DAC). (A) Support, (B) screws, (C) diamond anvils, (D) inconel gasket, (E) sample chamber. The main component of DAC is the two diamond anvils in opposing configuration which form the sample chamber with the metal gasket. By tightening the screws, the gasket is squeezed and the high pressure is generated with the reduction of the chamber volume.

2.2. Data acquisition at room temperature under atmospheric and elevated pressure

The diffraction data from CPMV crystals under high pressure were acquired at the Advanced Photon Source on the HP-CAT beamline at Sector 16. The wavelength was 0.4241 Å and the size of the beam was 100 × 100 µm, which was focused on a MAR 345 imaging-plate system. The crystal-to-detector distance was 1000.0 mm. Each exposure was made at a fresh area of the crystal with an oscillation angle of 0.3° for 10–30 s.

High pressure data collection was carried out with a cylindrical diamond anvil cell (DAC) (Fig. 2). An inconel gasket of 0.25 mm in thickness with a hole of 0.5 mm in diameter was used. Crystals of about 0.3 × 0.3 × 0.2 mm were chosen for the diffraction experiments. The pressure was ramped at 0.5 kbar intervals and calibrated with the ruby fluorescence with a spectrophotometer system (Betsa, Inc.).

The pressure medium was comprised of 55 m*M* potassium phosphate pH 7.0, 100 m*M* ammonium sulfate, 3% PEG 6K and 23% 2-methyl-2,4-pentanediol, which was a modification to reduce the viscosity from the medium previously used (Fourme *et al.*, 2002).

2.3. Data analysis

The program package *HKL* (Otwinowski & Minor, 1997) was used for the indexing, integration, scaling and merging of the reflection data.

2.4. Generation of synthetic data

A unit cell with dimensions of the *I*23 CPMV crystals was constructed by placing model virus particles (Lin *et al.,* 1999) at the

origin and the body center with the 2-, 3-symmetry elements of the icosahedra aligned with the tetrahedral point group at those positions. To simulate the disorder, the virus particle at the origin was rotated at half degree increments from 0 to 10° about the twofold axis coincident with Z while leaving the body centered particle invariant. Structure factors were calculated to 4 Å resolution after each rotation for comparison with the observed reflections.

3. Results and discussion

3.1. Integration of abnormal reflections at atmospheric pressure

Rhombic dodecahedral crystals of CPMV could be identified in two apparent space groups, $I23$ and $P23$. Past experience showed that over 90% of the crystals were associated with space group $P23$ owing to the appearance of reflections with indices of $h + k + l = (2n + 1)$ (odd reflections), which are forbidden in space group $I23$. To obtain data for both types of crystal, cryogenic techniques were adopted for data acquisition so that complete data sets could be collected once a crystal with an $I23$ space group was identified. A total six data sets were collected, one was shown to have perfect $I23$ packing (Data set No. 1 in Table 1) and the other five data sets were in the $P23$ space group (data sets Nos. 2–6 in Table 1).

Data set No. 1 contained 39 488 unique reflections (completeness 92.7%) in space group $I23$. The overall merged R factor was 5.5% (and 15% in the resolution shell from 4.07 to 4 Å). Data analysis showed that the scale factors relating data measured on individual frames correlated with the exponential decay of the current in the synchrotron radiation source. The intensity distribution of the data is shown in Fig. 3(*a*), which is normal for a typical macromolecular crystal.

For the reflections from the other five crystals, the data could be scaled and merged if the data processing was carried out in space group $I23$ with the exclusion of odd reflections. Data processing in the $P1$ or $P23$ space groups that included the odd reflections resulted in data sets that were poorly scaled when both scale factors and overall

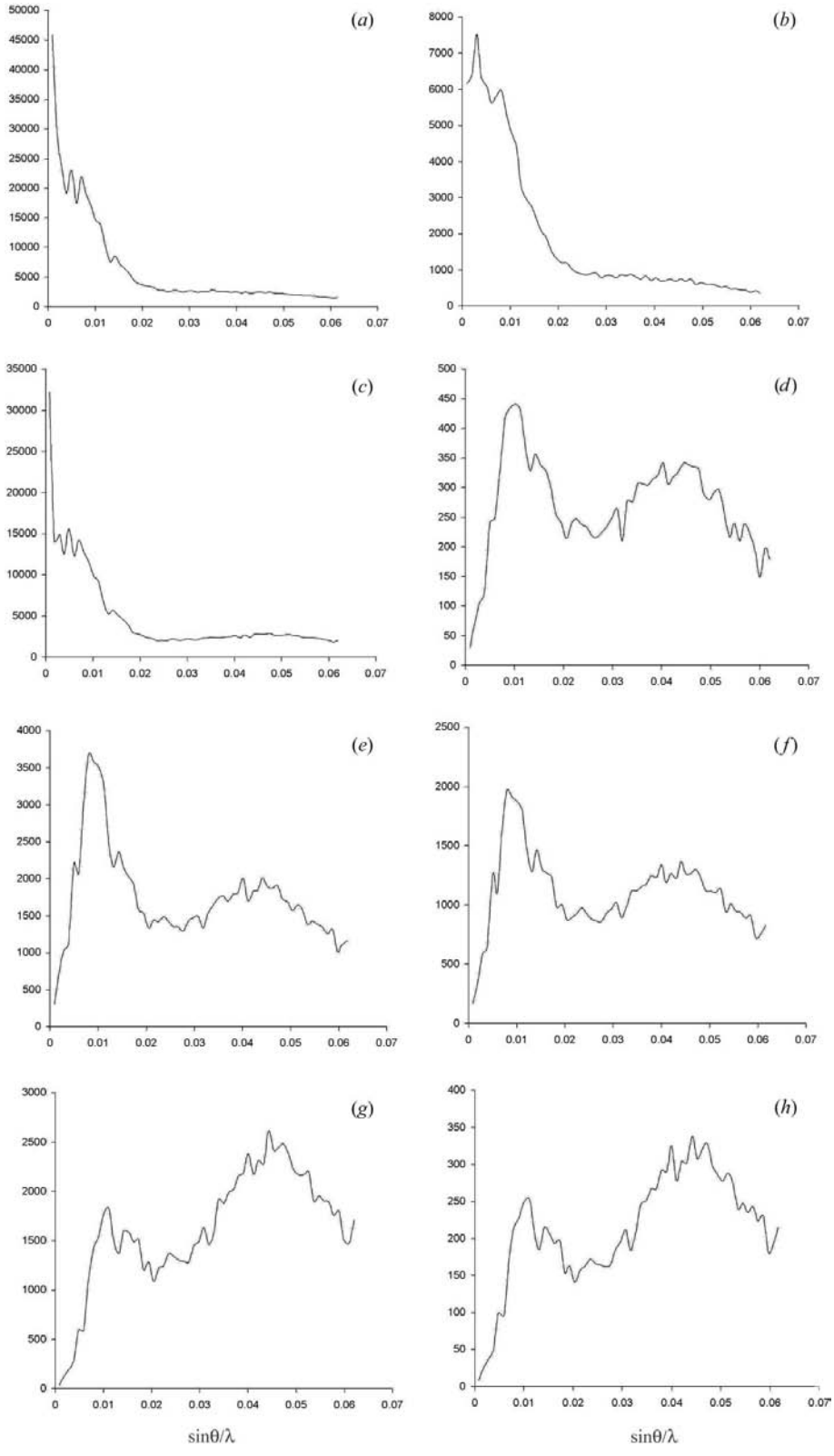

Figure 3
Plots of shells of averaged intensities *versus* $\sin\theta/\lambda$. Each data set is divided into 60 bins for the calculation of the average intensities. (*a*) Data set No. 1. The crystal is in space group $I23$ and the intensity distribution is typical for a macromolecular crystal. (*b*) The intensity distribution for reflections with indices of $(h + k + l) = 2n$ for data set No. 2. (*c*) Intensity distributions for reflections with indices of $(h + k + l) = 2n$ for data set No. 5. Similar intensity distributions were found for data sets No. 3, 4 and 6. (*d*) Density distribution for reflections with indices of $(h + k + l) = 2n+1$ (odd reflections) of data set No. 2. There are two maxima at the profile, one at about 10 Å ($\sin\theta/\lambda \simeq 0.01$) and the other at about 5 Å ($\sin\theta/\lambda \simeq 0.045$). The profile is similar to the synthetic data calculated from a model in which the origin particle is rotated by 2° from the standard orientation (see Fig. 4). (*e*)–(*h*). Intensity distribution of odd reflections from data sets No. 3–6. The rotational deviations are estimated as 3, 2.5, 1.5 and 1.5° for each crystal.

temperature factors were simultaneously refined. This was found to be the result of the unusual behavior of the odd reflections. They were weak at low resolution and increased in intensity with maxima at about 10 and 5 Å resolution which was inconsistent with a positive temperature factor. The scale factors also did not correlate to the decay of current in the synchrotron, which was contrary to the normal behavior observed in data set No. 1. These observations are consistent with a disorder in which virus particles behaving like spheres at low resolution show near *I*2 symmetry, but at high resolution, where the details of the subunit contribute to the diffraction pattern, the high symmetry breaks down.

To analyze the contribution of non-*I*23 reflections, a scheme was required to merge the frames into data sets with the *P*23 space group. A two-pass strategy was adopted. In the first pass, the data were merged in the *I*23 space group (*i.e.* odd reflections were ignored) and the temperature factors were determined for each frame. In the second pass, the temperature factors determined from the first were introduced as fixed values and the data were re-merged in the *P*23 space group (*i.e.* all data included). The intensity distribution of the even (those of indices $h + k + l = 2n$) and odd reflections was analyzed (Figs. 3*d*–3*h*). It is obvious that while the intensity distribution of even reflections is similar to those of typical macromolecular crystals (Figs. 3*b* and 3*c*), the intensity distribution of the odd reflections is abnormal.

3.2. Disorder as the origin of forbidden reflections in *I*23 space group

The abnormal intensity distribution of odd reflections is accompanied by diffuse scattering. Furthermore, the odd reflections were detrimental to scaling and the structure determination, indicating that they originated from particles that did not conform to the crystallographic order. Thus, the odd reflections are a consequence of disorder in crystal packing. The breakdown of *I*23 symmetry can be modeled by modification of each unit cell (Fig. 4). The modification is a rotation of the particle at the origin by an amount φ or $-\varphi$ around the twofold axis coincidental with z. In any particular unit cell there are equal chances of rotation by φ and by $-\varphi$ and the sign of the rotation is chosen independently for different unit cells. In different calculations, φ is selected from the range $0.5 \leq \varphi \leq 10^{\circ}$. The body-centered particle is invariant. We describe the unit cell contents as N spherical scatters distributed with icosahedral symmetry.

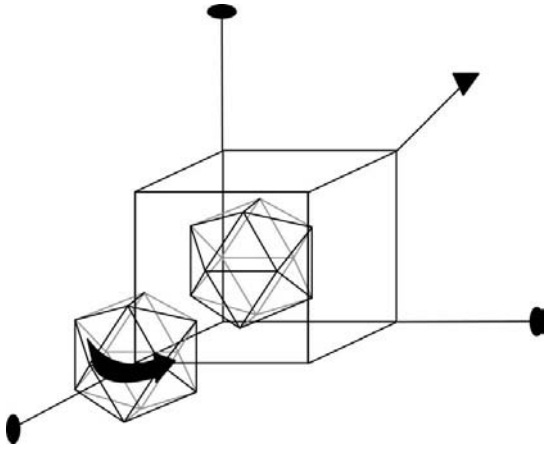

Figure 4
A model of the deviation of CPMV particle packing from the ideal *I*23 space group. The unit cell contains two virus particles at (0, 0, 0) and (1/2, 1/2, 1/2). The icosahedral twofold and threefold axes coincide with the crystallographic twofold and threefold axes. The forbidden odd reflections in space group *I*23 can be explained by a rotational deviation of the particle at the origin from the standard orientation.

The expression for the structure factor is

$$\mathbf{F}(\mathbf{H}) = \sum_{j=1}^{N} g_j(\mathbf{H}) \exp[i2\pi(\mathbf{H}\mathbf{R}_j)], \tag{1}$$

where $g_j(\mathbf{H})$ is the temperature-corrected atomic scattering factor which has the form

$$g_j(\mathbf{H}) = f_j(\mathbf{H}) T_j(\mathbf{H}), \tag{2}$$

where $f_j(\mathbf{H})$ is the atomic scattering factor and $T_j(\mathbf{H})$ is the temperature factor which has the form

$$T_j(\mathbf{H}) = \exp[-\mathbf{B}(\mathbf{H})(\sin^2\theta)/\lambda^2]. \tag{3}$$

The trigonometric expression for the structure factor $\mathbf{F}(\mathbf{H})$ is

$$\mathbf{F}(\mathbf{H}) = \sum_{j=1}^{N} g_j(\mathbf{H})[\cos 2\pi(\mathbf{H}\mathbf{R}_j) + i \sin 2\pi(\mathbf{H}\mathbf{R}_j)]. \tag{4}$$

In a body-centered cell, an atom at $\mathbf{R}$ is related by translation to another atom of the same type at $\frac{1}{2} + \mathbf{R}$. The structure-factor formulae (4), can be written as the sum for $N/2$ atoms:

$$\begin{aligned}
\mathbf{F}(\mathbf{H}) &= \sum_{j=1}^{N/2} g_j(\mathbf{H})\{[\cos 2\pi(\mathbf{H}\mathbf{R}_j) + i \sin 2\pi(\mathbf{H}\mathbf{R}_j)] \\
&\quad + [\cos 2\pi(\mathbf{H}(\mathbf{R}_j + \tfrac{1}{2}) + i \sin 2\pi\mathbf{H}(\mathbf{R}_j + \tfrac{1}{2})]\} \\
&= \sum_{j=1}^{N/2} g_j(\mathbf{H})\{[\cos 2\pi(\mathbf{H}\mathbf{R}_j) + i \sin 2\pi(\mathbf{H}\mathbf{R}_j)] \\
&\quad + [\cos 2\pi(\mathbf{H}\mathbf{R}_j)\cos(\pi\mathbf{H}) - \sin 2\pi(\mathbf{H}\mathbf{R}_j)\sin(\pi\mathbf{H}) \\
&\quad + i \sin 2\pi(\mathbf{H}\mathbf{R}_j)\cos(\pi\mathbf{H}) + i\cos 2\pi(\mathbf{H}\mathbf{R}_j)\sin(\pi\mathbf{H})]\}.
\end{aligned} \tag{5}$$

If the sum of the components of $\mathbf{H}$ is odd then

$$\begin{aligned}
\mathbf{F}_{\rm odd}(\mathbf{H}) &= \sum_{j=1}^{N/2} g_j(\mathbf{H})\{[\cos 2\pi(\mathbf{H}\mathbf{R}_j) + i \sin 2\pi(\mathbf{H}\mathbf{R}_j)] \\
&\quad + [\cos \pi\mathbf{H}(\mathbf{R}_j + \tfrac{1}{2}) + i \sin 2\pi\mathbf{H}(\mathbf{R}_j + \tfrac{1}{2})]\} \\
&= \sum_{j=1}^{N/2} g_j(\mathbf{H})\{[\cos 2\pi(\mathbf{H}\mathbf{R}_j) + i \sin 2\pi(\mathbf{H}\mathbf{R}_j)] \\
&\quad + [-\cos 2\pi(\mathbf{H}\mathbf{R}_j) - i \sin 2\pi(\mathbf{H}\mathbf{R}_j)]\} \\
&= 0.
\end{aligned} \tag{6}$$

(6) says that the systematic absence of the odd diffractions of body-centered cells results from cancellation of diffraction from the particles at (0, 0, 0) with the diffraction from those at (1/2, 1/2, 1/2).

Our model of disorder implies that the expected structure factor is

$$\begin{aligned}
\mathbf{F}(\mathbf{H}) = \sum_{j=1}^{N/2} g_j(\mathbf{H})\{&0.5[\cos 2\pi\mathbf{H}\mathbf{R}'_j + i \sin 2\pi\mathbf{H}\mathbf{R}'_j] \\
&+ 0.5[\cos 2\pi\mathbf{H}\mathbf{R}''_j + i \sin 2\pi\mathbf{H}\mathbf{R}''_j] \\
&+ [\cos 2\pi\mathbf{H}(\mathbf{R}_j + \tfrac{1}{2}) + i \sin 2\pi\mathbf{H}(\mathbf{R}_j + \tfrac{1}{2})]\},
\end{aligned} \tag{7}$$

where $\mathbf{R}'_j$ ($\mathbf{R}''_j$) is the location of the jth atom after the rotation by angle φ ($-\varphi$) around the twofold axis. If φ is small, which is the relevant case for the virus crystals, then $\mathbf{R}'_j = \mathbf{R}_j + \varphi\mathbf{z} \times \mathbf{R}_j$ and $\mathbf{R}''_j = \mathbf{R}_j - \varphi\mathbf{z} \times \mathbf{R}_j$ where $\times$ indicates vector cross product and $\mathbf{z}$ is a unit vector in the z direction.

Define $\Delta_j = \varphi\mathbf{z} \times \mathbf{R}_j$. Then (7) simplifies to

$$\begin{aligned}\mathbf{F}(\mathbf{H}) &= \sum_{j=1}^{N/2} g_j(\mathbf{H})\{0.5[\cos 2\pi\mathbf{H}(\mathbf{R}_j+\Delta_j) + i\sin 2\pi\mathbf{H}(\mathbf{R}_j+\Delta_j)] \\ &\quad + 0.5[\cos 2\pi\mathbf{H}(\mathbf{R}_j-\Delta_j) + \sin 2\pi\mathbf{H}(\mathbf{R}_j-\Delta_j)] \\ &\quad + [\cos 2\pi\mathbf{H}(\mathbf{R}_j+\tfrac{1}{2}) + i\sin 2\pi\mathbf{H}(\mathbf{R}_j+\tfrac{1}{2})]\} \qquad (8) \\ &= \sum_{j=1}^{N/2} g_j(\mathbf{H})\{\cos 2\pi\mathbf{H}\Delta_j[\cos 2\pi\mathbf{H}\mathbf{R}_j + i\sin 2\pi\mathbf{H}\mathbf{R}_j] \\ &\quad + [\cos 2\pi\mathbf{H}(\mathbf{R}_j+\tfrac{1}{2}) + i\sin 2\pi\mathbf{H}(\mathbf{R}_j+\tfrac{1}{2})]\}.\end{aligned}$$

The Taylor series of cos$Z$ is

$$\cos Z = 1 - Z^2/2! + Z^4/4! - \ldots,$$

so that if Z is small then

$$\cos Z = 1 - Z^2/2.$$

Applying this approximation to the $\cos 2\pi\mathbf{H}\Delta_j$ factor of (8) gives

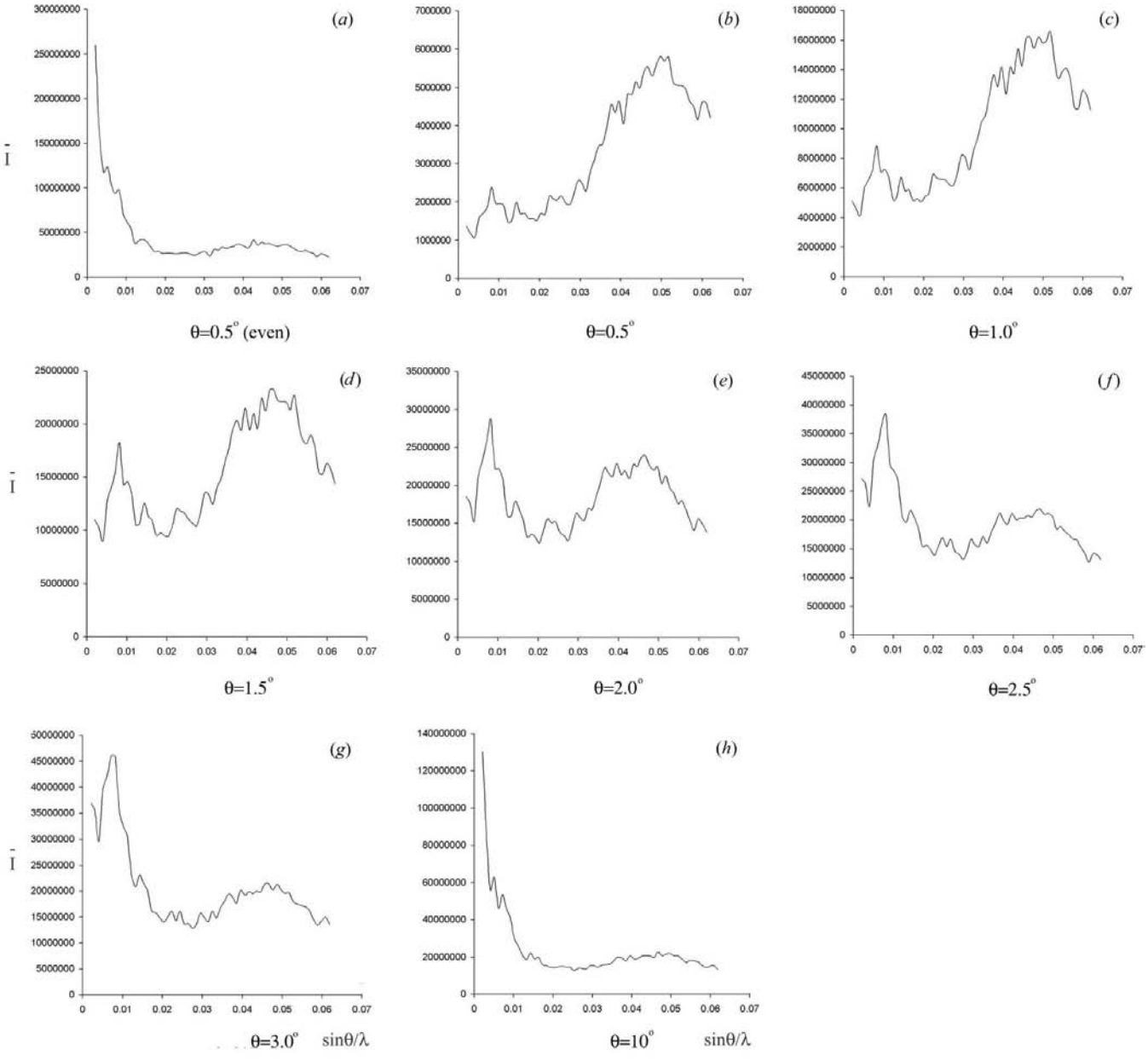

Figure 5
Plots of average intensity *versus* sinθ/λ for synthetic data sets. The calculated reflections in each data set are divided into 60 bins for the calculation of the average intensities. (*a*) The intensity distribution of even reflections from the model crystal in which the origin particle was rotated by 0.5°. The intensity distributions are similar for even reflections in all synthetic data sets, regardless of the degree of rotation in the origin particle. (*b*). Intensity distribution of odd reflections for the model crystal with the origin particle rotated by 0.5°. There are two peaks in the plot, one at about 10 Å (sin$\theta/\lambda \simeq 0.01$) and the other at 5 Å (sin$\theta/\lambda \simeq 0.045$). (*c*)–(*h*). Intensity distributions of odd reflections for model crystals with the origin particle rotated by 1.0, 1.5, 2, 2.5, 3.0 and 10°, respectively. Intensity distributions from other rotational deviations were also analyzed, but are not shown. The intensity distributions for models with origin particle rotated by 5–10° are similar. There is a change in the relative height between the peaks at 10 (sin$\theta/\lambda \simeq 0.01$) and 5 Å (sin$\theta/\lambda \simeq 0.045$) with increased rotational angle. The peak at 10 Å becomes higher with the larger rotational angle. When the rotational angles were sufficiently high (>5°), the intensity distribution behaved like a normal macromolecular crystal. By comparing the relative height of the two peaks, the synthetic data were used to estimate the rotational deviation of virus particles in the real crystals.

$$\mathbf{F}(\mathbf{H}) = \sum_{j=1}^{N/2} g_j(\mathbf{H})\{[\cos 2\pi\mathbf{H}\mathbf{R}_j + i\sin 2\pi\mathbf{H}\mathbf{R}_j] - [(2\pi\mathbf{H}\Delta_j)^2/2][\cos 2\pi\mathbf{H}\mathbf{R}_j + i\sin 2\pi\mathbf{H}\mathbf{R}_j] + [\cos 2\pi\mathbf{H}(\mathbf{R}_j + \tfrac{1}{2}) + i\sin 2\pi\mathbf{H}(\mathbf{R}_j + \tfrac{1}{2})]\}$$
$$= \mathbf{F}_{\rm perfect}(\mathbf{H}) + \sum_{j=1}^{N/2}[(2\pi\mathbf{H}\Delta_j)^2/2][\cos 2\pi\mathbf{H}\mathbf{R}_j + i\sin 2\pi\mathbf{H}\mathbf{R}_j],$$

where $\mathbf{F}_{\rm perfect}(\mathbf{H})$ is the function in (5).

If $\mathbf{H}$ is odd as in (6) then

$$\mathbf{F}(\mathbf{H}) = -\sum_{j=1}^{N/2} g_j(\mathbf{H})[(2\pi\mathbf{H}\Delta_j)^2/2][\cos 2\pi\mathbf{H}\mathbf{R}_j + i\sin 2\pi\mathbf{H}\mathbf{R}_j]$$

which is typically not zero.

It is a simplification to model all the disorder as occurring in the particles at the origin. A more realistic model is a statistical disorder distributed throughout the crystal. The mathematical treatment of this statistical model is beyond the scope of this manuscript and will be described in a separate article. However, this simplified model, as shown by the synthetic data below, adequately describes the origin of the odd reflections in *I*23 space group.

3.3. Synthetic reflection data simulating the disordering

Synthetic data sets were generated to simulate the disorder in *I*23 space group. A model was made by placing a refined virus capsid structure at the center of the unit cell in standard orientation (*i.e.* with icosahedral twofold and threefold axes coincide with the equivalent crystallographic axes), and another was placed at the origin with rotations from 0.5° to over 10°, in 0.5° increments (Fig. 4). The diffraction from the models were calculated and analyzed, as shown in Fig. 5.

The even reflections calculated from these models are similar to those for typical macromolecules (Fig. 5*a*). For the odd reflections, the highest intensity distribution is at the resolution of roughly 5 Å when the rotation angle is small (Fig. 5*b*). With the increase of rotation angles (Figs. 5*c*–5*f*), a second peak at about 10 Å is increasingly prominent in the intensity distribution plot. When the rotation angle is more than 5°, the intensity distribution is normal for all reflections (Fig. 5*h*).

Employing the model described, numerical calculation of the synthetic data simulates the disorder in CPMV *I*23 crystals as evidenced by comparing the intensity distribution between the real (Fig. 3) and synthetic data (Fig. 5). Based on matching the profiles of odd reflections between synthetic data (Figs. 5*b*–5*g*) and observed data (Figs. 3*d*–3*h*), it is estimated that the rotational deviation is about 2° for crystal No. 2, 3° for crystal No. 3, 2.5° for crystal No. 4, and 1.5° for crystals No. 5 and 6.

Table 2
Diffraction from a single frame of a CPMV crystal before and after pressure treatment.

	Atmospheric pressure	3.5 kbar pressure
Diffraction limits	3.0 Å resolution	2.1 Å resolution
Space group	*P*23	*I*23
Mosaicity	0.25°	0.1°
Data processing (25.0–3.0 Å)		
Total reflections	17867	5748
Full reflections	460	2012
$R_{\rm merge\ (\%)}$	Not determined	7.2

3.4. Pressure-dependent improvement of the crystal packing

At 3.5 kbar of pressure, all crystals displayed strict *I*23 symmetry, while the majority of crystals at atmospheric pressure are *P*23. To demonstrate that the pressure indeed induces a disorder–order transition, the diffraction pattern from one single crystal before and after the pressure treatment was measured for analysis (Fig. 1). At atmospheric pressure, this crystal diffracted X-rays to about 3 Å. The crystal could only be indexed with the *P*23 space group with a mosaicity of 0.25°. Treating the crystal with 3.5 kbar of pressure, the same crystal was readily indexed in the *I*23 space group. The crystal diffracted X-rays to about 2.1 Å and the mosaicity was reduced to 0.1°. The data processing before and after the pressure treatment is summarized in Table 2. The change of the apparent space group with the elimination of odd reflections and improvement in diffraction clearly demonstrates that pressure induces a correction of the disorder and transforms a crystal with defects to one with high order and associated enhanced diffraction power.

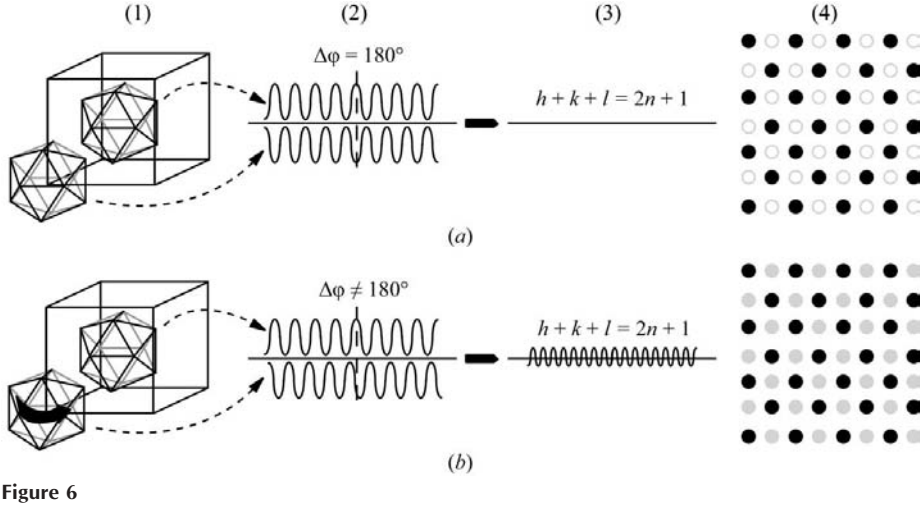

Figure 6
A mechanistic model of pressure-induced improvement of the imperfect CPMV crystals. (*a*) There are two virus particles in a perfect *I*23 cell (1), one at the origin and the other at the body center. (2) The odd reflections from the center have the same amplitudes but opposite phases to those from the origin, resulting in the systematic absence (3). (4) Schematic presentation of the precession photograph. The black circles represent the even reflections and the open circles represent the absent odd reflections. (*b*) A rotational deviation of the particles at the origin results in a shift of phases and the odd reflections are no longer absent, as represented in gray circles in the schematic precession photograph. The high pressure induces ordering by rectification of the rotational deviation and the crystals with the defects (*b*) are transformed to perfect *I*23 packing (*a*), which greatly improves the diffraction.

4. Conclusions

Most of the CPMV crystals had imperfections, which could be described as half the particles rotated from the standard orientation by 1.5–3°. This disorder was remedied by the application of hydrostatic pressure at 3.5 kbar. A mechanistic model is proposed on this pressure-induced ordering as shown in Fig. 6. It is likely that this phenomenon is not unique and improvement of diffraction by high pressure may be applicable to other macromolecular crystal systems.

The authors thank Dr Vukica Srajer for help in the data collection. The diffraction

data were acquired at beamlines of BioCARS (14-BMC) (NIH/NCRR No. 07707) and HP-CAT at Argonne National Laboratory. The help from Wendy Mao on the high pressure experiments is also gratefully acknowledged. This work was supported by grants from the Office of Naval Research to TL (N00014-03-1-0632) and JEJ (N00014-00-1-0671).

References

Fourme, R., Ascone, I., Kahn, R., Mezouar, M., Bouvier, P., Girard, E., Lin, T. & Johnson, J. E. (2002). *Structure*, **10**, 1409–1414.

Lin, T., Chen, Z., Usha, R., Stauffacher, C. V., Dai, J. B., Schmidt, T. & Johnson, J. E. (1999). *Virology*, **265**, 20–34.

Lomonossoff, G. P. & Johnson, J. E. (1991). *Prog. Biophys. Mol.* **55**, 107–137.

Otwinowski, Z. & Minor, W. (1997). *Methods Enzymol.* **276**, 307–326.

Stauffacher, C. V., Usha, R., Harrington, M., Schmidt, T., Hosur, M. & Johnson, J. E. (1987). *Crystallography in Molecular Biology*, edited by D. Moras, J. Drendt, B. Strandberg, D. Suck & K. Wilson, pp. 293–308. New York: Plenum Press.

Wikoff, W. R., Schildkamp, W. & Johnson, J. E. (2000). *Acta Cryst.* D**56**, 890–893.